UC Riverside
2018 Publications

Title
Pseudorange and multipath analysis of positioning with LTE secondary synchronization signals

Permalink
https://escholarship.org/uc/item/2dr336xp

Authors
Shamaei, K.
Khalife, J.
Kassas, Z.

Publication Date
2018-04-15

Peer reviewed

eScholarship.org Powered by the California Digital Library
University of California

Pseudorange and Multipath Analysis of Positioning with LTE Secondary Synchronization Signals

Kimia Shamaei, Joe Khalife, and Zaher M. Kassas
Department of Electrical and Computer Engineering
University of California, Riverside, USA
Emails: kimia.shamaei@email.ucr.edu,
jkhalife@ece.ucr.edu, zkassas@ieee.org

***Abstract*—The ranging precision of the long-term evolution (LTE) secondary synchronization signal (SSS) with noncoherent baseband discriminators is analyzed. The open-loop and closed-loop statistics of the code phase error with the dot-product and early-power-minus-late-power discriminator are derived. The effect of multipath on the code phase error is evaluated numerically. Experimental results demonstrating the efficacy of the derived statistics are presented, in which the total position root-mean squared error (RMSE) with SSS over a 560 m ground vehicle trajectory was reduced by 51%.**

I. Introduction

Cellular signals are exploitable for accurate navigation in environments where global navigation satellite systems (GNSS) signals are challenged [1], [2]. Cellular signals possess several desirable characteristics for positioning and navigation: abundance, favorable geometric transmitter configuration, high received power, large transmission bandwidth, and frequency diversity. Recent studies have focused on the fourth generation cellular standard, also known as long-term evolution (LTE), presenting software-defined receivers (SDRs) for LTE-based navigation [3]–[5] and demonstrating LTE-based navigation with meter-level accuracy [6]–[10].

The positioning performance of GPS signals has been well studied. However, extending these studies to LTE signals is not straightforward. LTE systems transmit using orthogonal frequency division multiplexing (OFDM), which is fundamentally different than GPS, which uses code-division multiple access (CDMA). There are two types of pilot signals in an OFDM system: (1) continual pilots and (2) scattered pilots. The achievable accuracy of the scattered pilot signals in OFDM systems has been evaluated in [11] and more specifically for positioning reference signals (PRS) and cell-specific reference signals (CRS) in LTE systems in [12]–[14]. The ranging precision of the continual pilots in LTE systems (i.e., the primary synchronization signal (PSS) and the secondary synchronization signal (SSS)) for a coherent delay-locked loop (DLL) has been analyzed in [15]. A coherent DLL can be used when the carrier phase tracking is ideal and the receiver's residual carrier phase and Doppler frequency are negligible. This paper focuses on analyzing the ranging precision of LTE's PSS and SSS signals with a noncoherent DLL, which avoids the dependency on carrier phase tracking.

This paper makes three contributions. First, the ranging precision of the SSS signal is evaluated for two noncoherent discriminator functions, namely a dot-product and an early-power-minus-late-power discriminator function. Second, the ranging error due to multipath is analyzed numerically. Third, experimental results of a ground vehicle navigating over a 560 m trajectory are presented showing that utilizing the derived pseudorange error variance into the estimator reduced the total positioning root-mean squared error (RMSE) by 51% and the positioning maximum error by 21%.

The remainder of the paper is organized as follows. Section II presents the received LTE signal model. Section III studies the open-loop statistics of the code phase error. Section IV derives the closed-loop statistics of the code phase error. Section V evaluates the code phase error in the presence of multipath. Section VI provides experimental results. Concluding remarks are given in Section VII.

II. Received LTE Signal Model

LTE signals are composed of frames with a duration of $T_{\text{sub}} = 10$ ms, where each frame consists 20 slots [16]. In each frame, two synchronization signals are transmitted to provide the user equipment (UE) the frame start time, namely the PSS and the SSS. The PSS can be one of three different orthogonal sequences determined by the sector ID of the eNodeB. The SSS can be one of 168 different orthogonal sequences determined by the group ID of the eNodeB. The UE can track all SSSs transmitted from the eNodeBs in the environment with sufficiently high carrier-to-noise ratios (C/N_0), which inherently increases the geometric diversity of tracked eNodeBs [4]. The SSS is transmitted only once in each frame, either in slot 0 or 10, and occupies the 62 middle subcarriers out of N_c total subcarriers. In LTE systems, N_c can only take values from the set $\{128, 256, 512, 1024, 1536, 2048\}$. The SSS signal is zero-padded to length N_c and an inverse Fourier transform (IFT) is taken according to

$$s_{\text{SSS}}(t) = \begin{cases} \text{IFT}\{S_{\text{SSS}}(f)\}, & \text{for } t \in (0, T_{\text{symb}}), \\ 0, & \text{for } t \in (T_{\text{symb}}, T_{\text{sub}}), \end{cases}$$

where $S_{\text{SSS}}(f)$ is the SSS sequence in the frequency-domain, $T_{\text{symb}} = 1/\Delta f$ is the duration of one symbol, and $\Delta f = 15$ KHz is the subcarrier spacing in LTE systems [16].

978-1-5386-1734-2/18/$31.00 ©2018 IEEE

The received signal is processed in blocks, each of which spans the duration of a frame, which can be modeled as

$$r(t) = \sqrt{C}e^{j(2\pi\Delta f_D t+\Delta\phi)} \cdot [s_{\text{code}}(t - t_{s_k} - kT_{\text{sub}}) + d(t - t_{s_k} - kT_{\text{sub}})] + n(t),$$
$$\text{for} \quad kT_{\text{sub}} \le t \le (k+1)T_{\text{sub}}, \quad k = 0, 1, 2, \cdots,$$

where $s_{\text{code}}(t) \triangleq \sqrt{\frac{T_{\text{sub}}}{W_{\text{SSS}}}} s_{\text{SSS}}(t)$; $W_{\text{SSS}} = 930$ KHz is the SSS bandwidth; C is the received signal power including antenna gains and implementation loss; t_{s_k} is the true time-of-arrival (TOA) of the SSS signal; $\Delta\phi$ and Δf_D are the residual carrier phase and Doppler frequency, respectively; $n(t)$ is an additive white noise with a constant power spectral density $N_0/2$ Watts/Hz; and $d(t)$ is some data transmitted by the eNodeB other than the SSS, where

$$d(t) = 0 \quad \text{for } t \notin (t_{s_k}, t_{s_k} + T_{\text{symb}}).$$

A frequency-locked loop (FLL)-assisted phase-locked loop (PLL) and a rate-aided DLL could be used to track the SSS. The DLL could employ a coherent or a noncoherent discriminator [17], [18]. Coherent discriminators are used when carrier phase tracking is ideal and the receiver's residual carrier phase and Doppler frequency are negligible ($\Delta\phi \approx 0$ and $\Delta f_D \approx 0$), while noncoherent discriminators are independent of carrier phase tracking.

In a typical DLL, the correlation of the received signal with the early, prompt, and late locally generated signals at time $t = kT_{\text{sub}}$ are calculated according to

$$Z_{x_k} = I_{x_k} + jQ_{x_k},$$

where x can be either e, p, or l representing early, prompt, or late correlations, respectively. Fig. 1 represents the general structure of the DLL.

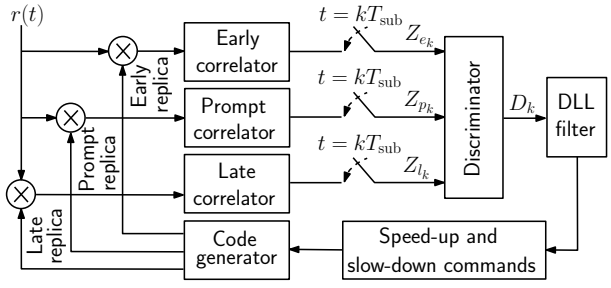

Fig. 1. General structure of the DLL to track the code phase.

Assuming the receiver's signal acquisition stage to provide a reasonably accurate estimate of f_D, the in-phase and quadrature components of the early, prompt, and late correlations can be written as

$$I_{x_k} = \sqrt{C}R\left(\Delta\tau_k + \kappa\frac{t_{\text{eml}}}{2}T_c\right)\cos(\Delta\phi_k) + \eta_{I,x_k},$$
$$Q_{x_k} = \sqrt{C}R\left(\Delta\tau_k + \kappa\frac{t_{\text{eml}}}{2}T_c\right)\sin(\Delta\phi_k) + \eta_{Q,x_k},$$

where x is e, p, or l and κ is -1, 0, or 1 for early, prompt, and late correlations, respectively; t_{eml} is the correlator spacing (early-minus-late); $\Delta\tau_k \triangleq \hat{t}_{s_k} - t_{s_k}$ is the propagation time estimation error; $\hat{t}_{s_k}$ and t_{s_k} are the estimated and the true TOA, respectively; and $R(\cdot)$ is the autocorrelation function of $s_{\text{code}}(t)$, given by

$$R(\Delta\tau) = \frac{1}{T_{\text{sub}}}\int_0^{T_{\text{sub}}} s_{\text{code}}(t)s_{\text{code}}(t+\Delta\tau)dt \approx \text{sinc}(W_{\text{SSS}}\Delta\tau).$$

It can be shown that the noise components η_{I,x_k} and η_{Q,x_k} of the correlations have: (1) uncorrelated in-phase and quadrature samples, (2) uncorrelated samples at different time, (3) zero-mean, and (4) the following variances and covariances

$$\text{var}\{\eta_{I,x_k}\} = \text{var}\{\eta_{Q,x_k}\} = \frac{N_0}{4T_{\text{sub}}}, \tag{1}$$
$$\mathbb{E}\{\eta_{I,e_k}\eta_{I,l_k}\} = \mathbb{E}\{\eta_{Q,e_k}\eta_{Q,l_k}\} = \frac{N_0R(t_{\text{eml}}T_c)}{4T_{\text{sub}}},$$
$$\mathbb{E}\{\eta_{I,x'_k}\eta_{I,p_k}\} = \mathbb{E}\{\eta_{Q,x'_k}\eta_{Q,p_k}\} = \frac{N_0R(\frac{t_{\text{eml}}}{2}T_c)}{4T_{\text{sub}}}, \tag{2}$$

where x' is e or l.

III. Open-Loop Statistics of the Code Phase Error

In this section, the open-loop statistics of the code phase error using dot-product and early-power-minus-late-power discriminators are analyzed.

A. Dot-Product Discriminator

The dot-product discriminator function is defined as

$$D_k \triangleq (I_{e_k} - I_{l_k})I_{p_k} + (Q_{e_k} - Q_{l_k})Q_{p_k} \triangleq S_k + N_k,$$

where S_k is the signal component of the dot-product discriminator given by

$$S_k = CR(\Delta\tau)\left\{R\left(\Delta\tau - \frac{t_{\text{eml}}}{2}T_c\right) - R\left(\Delta\tau + \frac{t_{\text{eml}}}{2}T_c\right)\right\},$$

and N_k is the noise component of the discriminator function, which has zero-mean. Fig. 2(a) shows the normalized S_k/C for $t_{\text{eml}} = \{0.25, 0.5, 1, 1.5, 2\}$. It can be seen that the signal component of the discriminator function is non-zero for $\Delta\tau/T_c > (1 + t_{\text{eml}}/2)$; which is in contrast to being zero for GPS C/A code with infinite bandwidth. This is due to the sinc autocorrelation function of the SSS versus the triangular autocorrelation function of the GPS C/A code.

For small values of $\Delta\tau_k$, the discriminator function can be approximated by a linear function according to

$$D_k \approx k_{\text{SSS}}\Delta\tau_k + N_k, \tag{3}$$

where $k_{\text{SSS}} \triangleq \left.\frac{\partial D_k}{\partial\Delta\tau_k}\right|_{\Delta\tau_k=0}$ and is given by

$$k_{\text{SSS}} = 4CW_{\text{SSS}}\left[\frac{\text{sinc}\left(\frac{t_{\text{eml}}}{2}\right) - \cos\left(\frac{\pi t_{\text{eml}}}{2}\right)}{t_{\text{eml}}}\right]. \tag{4}$$

The mean and variance of D_k are calculated to be

$$\mathbb{E}\{D_k\} = k_{\text{SSS}}\Delta\tau_k, \tag{5}$$
$$\text{var}\{D_k\} = \text{var}\{N_k\}\big|_{\Delta\tau_k=0} = \left(\frac{N_0^2}{4T_{\text{sub}}^2} + \frac{CN_0}{2T_{\text{sub}}}\right)[1 - R(t_{\text{eml}}T_c)]. \tag{6}$$

B. Early-Power-Minus-Late-Power Discriminator

The early-power-minus-late-power discriminator function is defined as

$$D_k \triangleq I_{e_k}^2 + Q_{e_k}^2 - I_{l_k}^2 - Q_{l_k}^2 \triangleq S_k + N_k,$$

where S_k can be shown to be

$$S_k = C\left\{R^2\left(\Delta\tau - \frac{t_{\text{eml}}}{2}T_c\right) - R^2\left(\Delta\tau + \frac{t_{\text{eml}}}{2}T_c\right)\right\},$$

and N_k is the noise component of the discriminator function, which has zero-mean. Fig. 2(b) shows the normalized S_k/C of the early-power-minus-late-power discriminator function for $t_{\text{eml}} = \{0.25, 0.5, 1, 1.5, 2\}$.

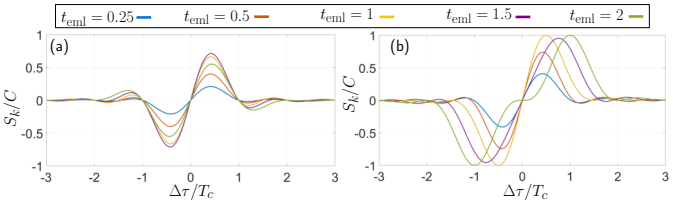

Fig. 2. Normalized signal component of (a) dot-product and (b) early-power-minus-late-power discriminator function for different correlator spacings.

The discriminator function can be approximated by a linear function for small values of $\Delta\tau_k$ (cf. (3)) with

$$k_{\text{SSS}} = 8CW_{\text{SSS}}R\left(\frac{t_{\text{eml}}}{2}T_c\right)\left[\frac{\text{sinc}\left(\frac{t_{\text{eml}}}{2}\right) - \cos\left(\frac{\pi t_{\text{eml}}}{2}\right)}{t_{\text{eml}}}\right]. \quad (7)$$

The mean and variance of D_k are calculated to be

$$\mathbb{E}\{D_k\} = k_{\text{SSS}}\Delta\tau_k, \quad (8)$$

$$\text{var}\{D_k\} = \frac{N_0^2}{2T_{\text{sub}}^2}\left[1 - R^2\left(t_{\text{eml}}T_c\right)\right] + \frac{2CN_0}{T_{\text{sub}}}R^2\left(\frac{t_{\text{eml}}}{2}T_c\right)\left[1 - R\left(t_{\text{eml}}T_c\right)\right]. \quad (9)$$

IV. Closed-Loop Statistics of the Code Phase Error

An FLL-assisted PLL produces reasonably accurate pseudorange rate estimate, making first-order DLLs sufficient. The closed-loop error time-update for a first-order loop can be shown to be

$$\Delta\tau_{k+1} = (1 - 4B_LT_{\text{sub}})\Delta\tau_k + K_LD_k,$$

where B_L is the loop noise bandwidth and K_L is the loop gain [17]. The loop noise bandwidth is achieved by normalizing the loop gain according to

$$K_L = \frac{4B_LT_{\text{sub}}\Delta\tau_k}{\mathbb{E}\{D_k\}}\Big|_{\Delta\tau_k=0}.$$

Therefore, using (5) and (8), the loop gain becomes

$$K_L = \frac{4B_LT_{\text{sub}}}{k_{\text{SSS}}}. \quad (10)$$

Assuming zero-mean tracking error, i.e., $\mathbb{E}\{\Delta\tau_k\} = 0$, the variance time-update can be computed to be

$$\text{var}\{\Delta\tau_{k+1}\} = (1 - 4B_LT_{\text{sub}})^2\text{var}\{\Delta\tau_k\} + K_L^2\text{var}\{D_k\}.$$

At steady-state, $\text{var}\{\Delta\tau\} = \text{var}\{\Delta\tau_{k+1}\} = \text{var}\{\Delta\tau_k\}$; hence,

$$\text{var}\{\Delta\tau\} = \frac{K_L^2}{8B_LT_{\text{sub}}(1 - 2B_LT_{\text{sub}})}\text{var}\{D_k\}. \quad (11)$$

In the following, the closed-loop statistics of the code phase error are derived for a dot-product and an early-power-minus-late-power discriminator functions.

A. Dot-Product Discriminator

The closed-loop code phase error in a dot-product discriminator can be obtained by substituting (4) and (6) into (11), yielding

$$\text{var}\{\Delta\tau\} = \frac{B_L\, g_\alpha(t_{\text{eml}})\left(1 + \frac{1}{2T_{\text{sub}}C/N_0}\right)}{16(1 - 2B_LT_{\text{sub}})W_{\text{SSS}}^2C/N_0}, \quad (12)$$

where

$$g_\alpha(t_{\text{eml}}) \triangleq \frac{t_{\text{eml}}^2\left[1 - R(t_{\text{eml}}T_c)\right]}{\left[\text{sinc}\left(t_{\text{eml}}/2\right) - \cos\left(\pi t_{\text{eml}}/2\right)\right]^2}.$$

Fig. 3(a) shows $g_\alpha(t_{\text{eml}})$ for $0 \le t_{\text{eml}} \le 2$. It can be seen that $g_\alpha(t_{\text{eml}})$ is a nonlinear function and increases significantly faster for $t_{\text{eml}} > 1$. Fig. 4 shows the standard deviation of the pseudorange error for a dot-product DLL as a function of C/N_0 with $t_{\text{eml}} = 1$ and $B_L = \{0.005, 0.05\}$ Hz, chosen as such in order to enable comparison with the GPS pseudorange error standard deviation provided in [15], [19].

B. Early-Power-Minus-Late-Power Discriminator

The variance of the ranging error in an early-power-minus-late-power discriminator can be obtained by substituting (7) and (9) into (11), yielding

$$\text{var}\{\Delta\tau\} = \frac{B_L\left[\frac{g_\beta(t_{\text{eml}})}{(C/N_0)} + 4T_{\text{sub}}g_\alpha(t_{\text{eml}})\right]}{64(1 - 2B_LT_{\text{sub}})T_{\text{sub}}W_{\text{SSS}}^2C/N_0}, \quad (13)$$

where

$$g_\beta(t_{\text{eml}}) \triangleq \frac{1 + R\left(t_{\text{eml}}T_c\right)}{R^2\left(\frac{t_{\text{eml}}}{2}T_c\right)}g_\alpha(t_{\text{eml}}).$$

Fig. 3(b) shows $g_\beta(t_{\text{eml}})$ for $0 \le t_{\text{eml}} \le 2$. It can be seen that $g_\beta(t_{\text{eml}})$ is significantly larger than $g_\alpha(t_{\text{eml}})$. To reduce the ranging error due to $g_\beta(t_{\text{eml}})$, t_{eml} must be chosen to be less than 1.5.

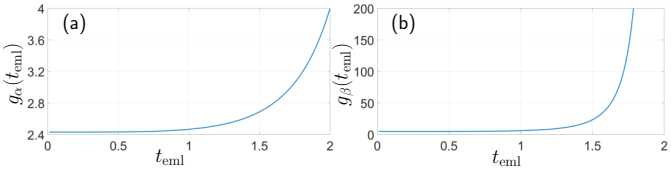

Fig. 3. The variance of the ranging error in a dot-product discriminator is related to the correlator spacing through $g_\alpha(t_{\text{eml}})$ shown in (a), while for an early-power-minus-late-power discriminator it is related through $g_\alpha(t_{\text{eml}})$ and $g_\beta(t_{\text{eml}})$ shown in (b).

Fig. 4 shows the standard deviation of the pseudorange error for an early-power-minus-late-power discriminator DLL as a function of C/N_0 with $B_L = \{0.05, 0.005\}$ Hz and $t_{\text{eml}} = 1$. It can be seen that decreasing the loop bandwidth decreases the standard deviation of the pseudorange error. However, very small values of B_L may cause the DLL to lose lock in a highly dynamic scenario.

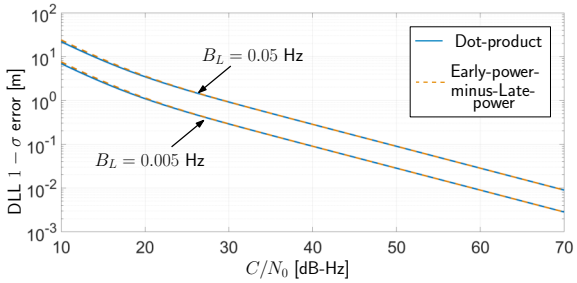

Fig. 4. DLL performance as a function of C/N_0 for a dot-product discriminator (solid line) and an early-power-minus-late-power discriminator (dashed line), $B_L = \{0.05, 0.005\}$ Hz, and $t_{\text{eml}} = 1$.

V. Code Phase Error Analysis in Multipath Environments

This section analyzes the code phase error in two types of multipath environments. In a multipath environment, the received signal can be modeled as

$$r(t) = \sum_{l=0}^{L-1} \alpha_l(t) y(t - \tau_l(t)) + n(t), \tag{14}$$

where $\alpha_l(t)$ and $\tau_l(t)$ are the channel's path complex gain and delay of the l-th path at time t, respectively; L is the total number of paths; and $y(t)$ is the transmitted data. A multipath channel will attenuate the discriminator function and the amount of attenuation depends on α_l and τ_l. It is important to note that an analytical closed-form expression for the pseudorange error in the presence of multipath is intractable for a noncoherent discriminator. Therefore, in what follows, numerical simulations will be used to characterize the performance of SSS code phase tracking with DLLs employing dot-product and early-power-minus-late-power discriminators.

The first multipath environment considers a channel with only one multipath component, where the multipath signal amplitude is 6 dB lower than the line-of-sight (LOS) signal amplitude. The effect of τ_1, the delay of the reflected signal, on the pseudorange estimation performance is evaluated for constructive and destructive interference. Since the goal is to assess the ranging performance in a multipath environment, no noise was added to the simulated signals. The zero crossing point of the discriminator function was calculated using Newton's method. The resulting pseudorange error for a dot-product discriminator is shown in Fig. 5 as a function of the relative path delay (in meters) for $t_{\text{eml}} = \{0.25, 0.5, 1, 1.5\}$. It was noted that the pseudorange errors for the early-power-minus-late-power discriminator were very close (within a few millimeters) to the plots in Fig. 5 for the same t_{eml} settings.

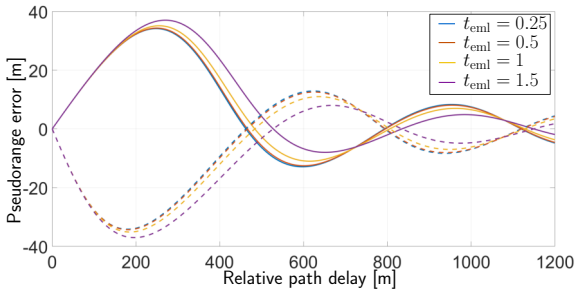

Fig. 5. Pseudorange error for a dot-product discriminator for a channel with one multipath component with an amplitude that is 6 dB lower than the amplitude of the LOS signal. The error is plotted as a function of the path delay (in meters) and for different t_{eml} values. The solid and dashed lines represent constructive and destructive interferences, respectively. Pseudorange errors for an early-power-minus-late-power discriminator are almost identical.

It can be seen from Fig. 5 that the pseudorange error is not zero-valued for high relative path delays. This is due to the sinc autocorrelation function of the SSS signal. In contrast, the autocorrelation function of the GPS C/A code has a triangular shape, which is zero-valued for time delays greater than T_c. Therefore, no multipath errors will be introduced in the pseudorange for multipath with relative delay greater than $(1 + t_{\text{eml}}/2)T_c$.

The second multipath environment considers three evolved universal terrestrial radio access (E-UTRA) channel models: extended pedestrian A (EPA), extended vehicular A (EVA), and extended typical urban (ETU) [20]. To asses the performance of the DLL in each channel, 10^5 random realizations of each channel were generated and the corresponding pseudorange errors were computed. Table I shows the mean μ and standard deviation σ of the pseudorange error for each of the E-UTRA channels and for the two discriminators under study. Note that similar results were obtained for $0 \leq t_{\text{eml}} \leq 1.5$.

Table I shows that the dot-product discriminator slightly outperforms the early-power-minus-late-power discriminator. The bandwidth of the SSS (930 KHz) makes it susceptible to multipath-induced error, causing the accuracy of the estimated position from the standalone SSS signal to be not satisfactory in certain environments. Several methods could be used to circumvent this, including using multipath mitigation algorithms, fusing with inertial sensors, and exploiting other LTE reference signals with higher transmission bandwidth (e.g., cell-specific reference signal) [5], [21].

VI. Experimental Results

This section presents experimental results of a ground vehicle estimating its trajectory from SSS signals, utilizing the pseudorange error statistics derived in Section IV.

A. Pseudorange Model and Navigation Framework

This subsection discusses the pseudorange model and the position estimators used in the experiments, namely nonlinear least-squares (NLS) and weighted NLS (WNLS) estimators.

1) Pseudorange Model: By multiplying the TOA estimated by the LTE receiver by the speed-of-light c, a pseudorange

TABLE I
PSEUDORANGE ERROR (IN METERS) DUE TO MULTIPATH FOR E-UTRA CHANNELS WITH $t_{\text{eml}} = 1$

Channel	EPA		ETU		EVA	
Discriminator	μ	σ	μ	σ	μ	σ
Dot-Product	12.72	21.34	62.97	66.06	57.64	69.91
Early-Power-Minus-Late-Power	12.65	21.03	64.51	65.29	59.45	70.81

measurement to each eNodeB can be obtained, which is modeled according to

$$\rho_i(k) = \|\boldsymbol{r}_r(k) - \boldsymbol{r}_{s_i}\|_2 + c\delta t_i(k) + v_i(k), \quad i = 1, \ldots, N,$$

where $\boldsymbol{r}_r \triangleq [x_r, y_r]^{\mathsf{T}}$ and $\boldsymbol{r}_{s_i} \triangleq [x_{s_i}, y_{s_i}]^{\mathsf{T}}$ are the two-dimensional (2D) position vectors of the receiver and the ith eNodeB, respectively; δt_i is the clock bias difference between the receiver and the ith eNodeB clocks; v_i is the measurement noise, which is modeled as a zero-mean white Gaussian random variable with variance σ_i^2; and N is the total number of eNodeBs.

It has been shown that the clock biases can be estimated on-the-fly and removed from the pseudoranges using an extended Kalman filter (EKF) or a mapper/navigator framework [22], [23]. Evaluating the effect of the clock stability is out of scope of this paper. Therefore, the clock biases were assumed to drift at a constant rate, i.e., $c\delta t_i(t) = a_i t + b_i$. The first few pseudorange measurements, the known eNodeB positions, and the initial receiver position obtained from GPS were used to estimate the coefficients $\{a_i, b_i\}_{i=1}^N$. Subsequently, a range measurement is defined according to

$$z_i(k) \triangleq \rho_i(k) - (a_i k T_{\text{sub}} + b_i) = \|\boldsymbol{r}_r(k) - \boldsymbol{r}_{s_i}\|_2 + v_i(k).$$

2) NLS and WNLS Estimators: Two estimators were used to estimate the position of the receiver: NLS and WNLS. Both estimators produced an estimate of the receiver's position at each time-step k using the measurements $\{z_i(k)\}_{i=1}^N$, where $N \geq 2$. The weighting matrix in the WNLS was

$$\mathbf{W}^{-1} = c^2 \cdot \text{diag}\left[\text{var}\{\Delta\tau_1\}, \ldots, \text{var}\{\Delta\tau_N\}\right],$$

where $\text{var}\{\Delta\tau_i\}$ was computed from (12). Subsequently, the position estimate $\hat{\boldsymbol{r}}_r$ at time-step k was obtained using the standard NLS and WNLS iterative equations, given by

$$\hat{\boldsymbol{r}}_r^{(u+1)} = \hat{\boldsymbol{r}}_r^{(u)} + \left(\mathbf{H}^{\mathsf{T}}\mathbf{H}\right)^{-1}\mathbf{H}^{\mathsf{T}}\boldsymbol{\nu}^{(u)},$$
$$\hat{\boldsymbol{r}}_r^{(u+1)} = \hat{\boldsymbol{r}}_r^{(u)} + \left(\mathbf{H}^{\mathsf{T}}\mathbf{W}\mathbf{H}\right)^{-1}\mathbf{H}^{\mathsf{T}}\mathbf{W}\boldsymbol{\nu}^{(u)},$$

respectively, where u is the iteration number and

$$\mathbf{H} \triangleq \left[\frac{\hat{\boldsymbol{r}}^{(u)} - \boldsymbol{r}_{s_1}}{\left\|\hat{\boldsymbol{r}}^{(u)} - \boldsymbol{r}_{s_1}\right\|_2}, \ldots, \frac{\hat{\boldsymbol{r}}^{(u)} - \boldsymbol{r}_{s_N}}{\left\|\hat{\boldsymbol{r}}^{(u)} - \boldsymbol{r}_{s_N}\right\|_2}\right]^{\mathsf{T}},$$
$$\boldsymbol{\nu}^{(u)} \triangleq \left[\nu_1^{(u)}, \ldots, \nu_N^{(u)}\right]^{\mathsf{T}}, \ \nu_i^{(u)} \triangleq z_i(k) - \left\|\hat{\boldsymbol{r}}^{(u)} - \boldsymbol{r}_{s_i}\right\|_2.$$

B. Experimental Setup

A ground vehicle was equipped with two consumer-grade cellular antennas to receive LTE signals at 739 MHz and 1955 MHz carrier frequencies used by the U.S. LTE provider AT&T. A dual-channel universal software radio peripheral (USRP) was used to simultaneously down-mix and synchronously sample LTE signals at 20 Msps. The vehicle was also equipped with one GPS antenna to receive C/A L1 signals, which were down-mixed and sampled by a single-channel USRP. The GPS signals were used to produce the vehicle's "ground truth." Samples of the LTE and GPS signals were stored for post-processing. LTE signals were processed and pseudoranges were obtained using the Multichannel Adaptive TRansceiver Information eXtractor (MATRIX) SDR, developed at the Autonomous Systems Perception, Intelligence, and Navigation (ASPIN) Laboratory at the University of California, Riverside [4]. GPS signals from 10 satellites were processed using the Generalized Radionavigation Interfusion Device (GRID) SDR [24]. Fig. 6 shows the experimental setup.

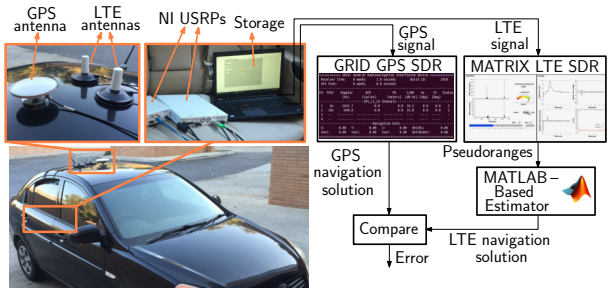

Fig. 6. Experimental setup.

C. Positioning Results

Over the 560 m course of the experiment, the receiver was listening to 4 eNodeBs whose positions $\{\boldsymbol{r}_{s_i}\}_{i=1}^4$ were mapped prior to the experiment. The pseudorange errors were obtained by subtracting the pseudoranges and their corresponding actual ranges. The initial values of the pseudorange errors, which were assumed to be due to the clock biases were removed. The pseudorange errors showed average of -2.12, -7.46, 4.08, 13.50 m and standard deviation of 6.71, 3.93, 1.75, 5.93 m for eNodeBs 1–4, respectively. The errors attributed to several factors including: (1) multipath, (2) clock drift, and (3) noise. The overall CIR over the course of the experiment had less multipath compared to the E-UTRA channel models and as a result the pseudorange errors' means and standard deviations are lower than the results shown in Table I.

The NLS and WNLS estimators described in Subsection VI-A were used to estimate the receiver's position from the same set of LTE pseudoranges. The experiment layout, the receiver's true trajectory, and the WNLS and NLS estimated trajectories are shown in Fig. 7, along with the total position RMSEs and maximum errors.

It can be seen that the WNLS produced a much closer estimated trajectory to the GPS trajectory than the one produced by the NLS, which did not incorporate the statistics of the pseudorange error. Incorporating (12) into the estimator

reduced the total RMSE by 51% and the position maximum error by 21%. The objective of these experimental results was to demonstrate the efficacy of (12). A more sophisticated dynamic estimator could be used to properly model the clock bias and drift dynamics (oscillator stability) [25] and a smoother estimated trajectory could be obtained by fusing the pseudoranges with an inertial sensor [10], [26]–[28].

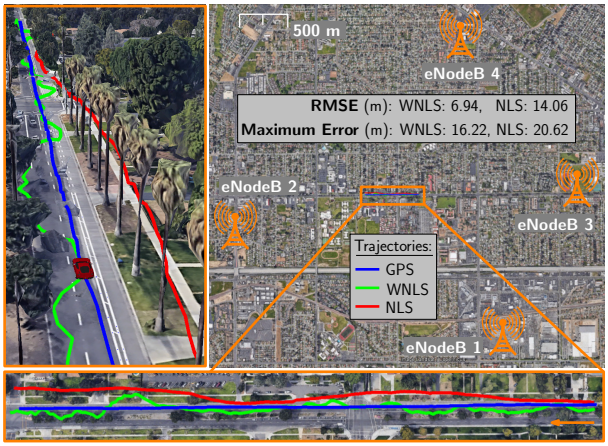

Fig. 7. Experimental results for positioning with LTE SSS signals in downtown Riverside, California, using: (i) WNLS estimator whose weights were calculated to (12) and (ii) NLS estimator. The position errors are calculated with respect to the GPS solution. Image: Google Earth.

VII. Conclusions

The ranging precision of the SSS signal in an additive white Gaussian noise channel and in a multipath environment was evaluated. The open-loop and closed-loop statistics of the error were obtained for two noncoherent baseband discriminators: dot-product and early-power-minus-late-power. Experimental results showed that using the derived statistics of the pseudo-range error significantly improves the estimated position.

Acknowledgment

This work was supported in part by the Office of Naval Research (ONR) under Grant N00014-16-1-2305.

References

[1] C. Yang, T. Nguyen, and E. Blasch, "Mobile positioning via fusion of mixed signals of opportunity," *IEEE Aerospace and Electronic Systems Magazine*, vol. 29, no. 4, pp. 34–46, April 2014.

[2] Z. Kassas, J. Khalife, K. Shamaei, and J. Morales, "I hear, therefore I know where I am: Compensating for GNSS limitations with cellular signals," *IEEE Signal Processing Magazine*, pp. 111–124, September 2017.

[3] J. del Peral-Rosado, J. Lopez-Salcedo, G. Seco-Granados, F. Zanier, P. Crosta, R. Ioannides, and M. Crisci, "Software-defined radio LTE positioning receiver towards future hybrid localization systems," in *Proceedings of International Communication Satellite Systems Conference*, October 2013, pp. 14–17.

[4] K. Shamaei, J. Khalife, and Z. Kassas, "Performance characterization of positioning in LTE systems," in *Proceedings of ION GNSS Conference*, September 2016, pp. 2262–2270.

[5] K. Shamaei, J. Khalife, S. Bhattacharya, and Z. Kassas, "Computationally efficient receiver design for mitigating multipath for positioning with LTE signals," in *Proceedings of ION GNSS Conference*, September 2017, pp. 3751–3760.

[6] C. Gentner, E. Munoz, M. Khider, E. Staudinger, S. Sand, and A. Dammann, "Particle filter based positioning with 3GPP-LTE in indoor environments," in *Proceedings of IEEE/ION Position, Location and Navigation Symposium*, April 2012, pp. 301–308.

[7] F. Knutti, M. Sabathy, M. Driusso, H. Mathis, and C. Marshall, "Positioning using LTE signals," in *Proceedings of Navigation Conference in Europe*, April 2015, pp. 1–8.

[8] M. Driusso, C. Marshall, M. Sabathy, F. Knutti, H. Mathis, and F. Babich, "Vehicular position tracking using LTE signals," *IEEE Transactions on Vehicular Technology*, vol. 66, no. 4, pp. 3376–3391, April 2017.

[9] M. Ulmschneider and C. Gentner, "Multipath assisted positioning for pedestrians using LTE signals," in *Proceedings of IEEE/ION Position, Location, and Navigation Symposium*, April 2016, pp. 386–392.

[10] K. Shamaei, J. Khalife, and Z. Kassas, "Comparative results for positioning with secondary synchronization signal versus cell specific reference signal in LTE systems," in *Proceedings of ION International Technical Meeting Conference*, January 2017, pp. 1256–1268.

[11] P. Thevenon, S. Damien, O. Julien, C. Macabiau, M. Bousquet, L. Ries, and S. Corazza, "Positioning using mobile TV based on the DVB-SH standard," *NAVIGATION, Journal of the Institute of Navigation*, vol. 58, no. 2, pp. 71–90, 2011.

[12] J. del Peral-Rosado, J. Lopez-Salcedo, G. Seco-Granados, F. Zanier, and M. Crisci, "Analysis of positioning capabilities of 3GPP LTE," in *Proceedings of ION GNSS Conference*, September 2012, pp. 139–146.

[13] J. del Peral-Rosado, J. Lopez-Salcedo, G. Seco-Granados, F. Zanier, and M. Crisci, "Evaluation of the LTE positioning capabilities under typical multipath channels," in *Proceedings of Advanced Satellite Multimedia Systems Conference and Signal Processing for Space Communications Workshop*, September 2012, pp. 139–146.

[14] M. Huang and W. Xu, "Enhanced LTE TOA/OTDOA estimation with first arriving path detection," in *Proceedings of IEEE Wireless Communications and Networking Conference*, April 2013, pp. 3992–3997.

[15] K. Shamaei, J. Khalife, and Z. Kassas, "Ranging precision analysis of LTE signals," in *Proceedings of European Signal Processing Conference*, August 2017, pp. 2788–2792.

[16] 3GPP, "Evolved universal terrestrial radio access (E-UTRA); physical channels and modulation," 3rd Generation Partnership Project (3GPP), TS 36.211, January 2011. [Online]. Available: http://www.3gpp.org/ftp/Specs/html-info/36211.htm

[17] A. van Dierendonck, P. Fenton, and T. Ford, "Theory and performance of narrow correlator spacing in a GPS receiver," *NAVIGATION, Journal of the Institute of Navigation*, vol. 39, no. 3, pp. 265–283, September 1992.

[18] M. Braasch and A. van Dierendonck, "GPS receiver architectures and measurements," *Proceedings of the IEEE*, vol. 87, no. 1, pp. 48–64, January 1999.

[19] P. Misra and P. Enge, *Global Positioning System: Signals, Measurements, and Performance*, 2nd ed. Ganga-Jamuna Press, 2010.

[20] 3GPP, "Evolved universal terrestrial radio access (E-UTRA); user equipment (UE) radio transmission and reception," 3rd Generation Partnership Project (3GPP), TS 136.101, June 2011. [Online]. Available: http://www.3gpp.org/ftp/Specs/html-info/36212.htm

[21] F. Dovis, M. Pini, and P. Mulassano, "Multiple DLL architecture for multipath recovery in navigation receivers," in *Proceedings of Vehicular Technology Conference*, vol. 5, May 2004, pp. 2848–2851.

[22] J. Khalife and Z. Kassas, "Navigation with cellular CDMA signals – part II: Performance analysis and experimental results," *IEEE Transactions on Signal Processing*, 2017, accepted.

[23] K. Shamaei, J. Khalife, and Z. Kassas, "Exploiting LTE signals for navigation: Theory to implementation," *IEEE Transactions on Wireless Communications*, 2017, accepted.

[24] T. Humphreys, J. Bhatti, T. Pany, B. Ledvina, and B. O'Hanlon, "Exploiting multicore technology in software-defined GNSS receivers," in *Proceedings of ION GNSS Conference*, September 2009, pp. 326–338.

[25] Z. Kassas and T. Humphreys, "Observability analysis of collaborative opportunistic navigation with pseudorange measurements," *IEEE Transactions on Intelligent Transportation Systems*, vol. 15, no. 1, pp. 260–273, February 2014.

[26] Y. Sun, Y. Zhao, and J. Schiller, "An indoor positioning system based on inertial sensors in smartphone," in *Proceedings of IEEE Wireless Communications and Networking Conference*, March 2015, pp. 2221–2226.

[27] J. Morales, P. Roysdon, and Z. Kassas, "Signals of opportunity aided inertial navigation," in *Proceedings of ION GNSS Conference*, September 2016, pp. 1492–1501.

[28] Z. Kassas, J. Morales, K. Shamaei, and J. Khalife, "LTE steers UAV," *GPS World Magazine*, vol. 28, no. 4, pp. 18–25, April 2017.